J. Fluid Mech. (1999), *vol.* 384, *pp.* 243–262. Printed in the United Kingdom

Convective versus absolute instability in mixed Rayleigh–Bénard–Poiseuille convection

By PHILIPPE CARRIÈRE[1] AND PETER A. MONKEWITZ[2]

[1]Laboratoire de Mécanique des Fluides et d'Acoustique, UMR CNRS 5509, Ecole Centrale de Lyon-Université Claude Bernard Lyon I, BP163, 69131 Ecully cedex, France
[2]IMHEF-Laboratoire de Mécanique des Fluides, Ecole Polytechnique Fédérale de Lausanne, CH-1015, Lausanne, Switzerland

(Received 4 April 1998 and in revised form 7 September 1998)

Transition from convective to absolute instability in Rayleigh–Bénard convection in the presence of a uni-directional Poiseuille flow is studied. The evaluation of the long-time behaviour of the Green function in the horizontal plane allows the determination of regions of convective and absolute instability in the Rayleigh–Reynolds number plane as a function of Prandtl number. It is found that the mode reaching zero group velocity at the convective–absolute transition always corresponds to transverse rolls, while the system remains convectively unstable with respect to pure streamwise (longitudinal) rolls for all non-zero Reynolds numbers. Finally, the roll pattern within the entire wave packet and in particular near its centre is elucidated and possible connections between experiments and our findings are discussed.

1. Introduction

The present study takes a closer look at the transition from convective to absolute instability of a Rayleigh–Bénard cell with a superimposed plane Poiseuille flow (henceforth abbreviated as the RBP system). The concept of convective and absolute instability, originally introduced by Briggs (1964) and applied to hydrodynamic instabilities by Huerre & Monkewitz (1985), among others, has often a direct bearing on the manifestation of an instability. In short, the concept is based on the long-time behaviour of the impulse response at a fixed spatial location: if it decays, the flow is stable or convectively unstable; if it is unbounded (within the context of linear theory), one speaks of absolute instability. As a consequence, a convective instability needs to be excited continuously to remain manifest at a fixed location, thus making the resulting perturbation in general excitation dependent. In an absolutely unstable flow, on the other hand, different initial excitations normally lead to the same intrinsic perturbation pattern at any fixed location. Since the primary instability in pure Rayleigh–Bénard (RB) convection is known to be absolute and pure plane Poiseuille flow is convectively unstable (Deissler 1987), it is expected that the nature of the instability in the mixed flow depends on the value of the three control parameters: the Rayleigh number ($\mathscr{R}$), Reynolds number (R) and Prandtl number (P). This system is therefore of interest for future experimental studies aimed at elucidating the physical manifestations of the convective–absolute transition in systems with two wave-propagation directions.

At this point, we briefly recall the salient features of the RBP stability problem which trivially reduces to the classical Rayleigh–Bénard problem for zero Reynolds

number and to the Orr–Sommerfeld problem for zero Rayleigh number. In both limit cases, the classical stability boundary is defined in a space of only two parameters: the Rayleigh or Reynolds number and a single wavenumber because the RB problem is invariant with respect to rotations in the horizontal plane and the Orr–Sommerfeld problem can be Squire transformed. The linear stability of the mixed RBP system was first investigated by Gage & Reid (1968). In this case, the stability properties depend in general on five parameters: $\mathscr{R}$, R, P and the two components a (in the flow direction x) and b (in the transverse direction y) of the wavevector. Inspection of the governing equations shows that simplifications arise for wave vectors orthogonal to the mean flow direction, as the stability boundary for these so-called *longitudinal* rolls (LRs) is independent of the Reynolds number. In other words, the critical parameters for LRs are the same as in the RB problem, namely $\mathscr{R}_c = \mathscr{R}_c^{(RB)} \approx 1707.76$ and $b_c \approx 3.116$. For oblique rolls, Gage & Reid (1968) have devised a Squire-type transformation which allows an analysis of the classical linear RBP stability problem in terms of LRs and TRs (transverse rolls with wavevector in the mean flow direction) alone. More recently, Müller (1990) and Müller, Lücke & Kamps (1992) have analysed TRs for small Reynolds numbers using an expansion in powers of R^2. Their main results are that the TRs become travelling rolls for non-zero R and that the increase of the critical Rayleigh number beyond $\mathscr{R}_c^{(RB)}$ is proportional to R^2 with a complicated dependence of the coefficient on P. Although we will focus in this paper on low Reynolds numbers of $O(10)$ at most, we mention in passing the results of Fujimura & Kelly (1995) at high Reynolds numbers who documented the appearance of a transverse Tollmien–Schlichting mode for $R > 140$ (at $P = 1$). In summary, the linear stability analyses have established that, for non-zero Reynolds number and fixed values of the Rayleigh and Prandtl numbers, LRs exhibit the highest temporal growth rate, while flow stabilizes the travelling TRs. A detailed review of the problem has recently been given by Kelly (1994).

From the above result it is usually concluded that longitudinal roll patterns are preferred in supercritical mixed convection. In many experimental studies (Akiyama, Hwang & Cheng 1971; Ostrach & Kamotani 1975; Fukui, Nakajima & Hueda 1983, for instance) supercritical longitudinal rolls have indeed been observed. However, some authors also reported observing transverse rolls (Luijkx, Platten & Legros 1981; Ouazzani *et al.* 1989; Ouazzani, Platten & Mojtabi 1990) depending on the values of the Rayleigh number and (low enough) Reynolds number. One possible explanation is the convective–absolute transition referred to above. To our knowledge, only a few studies have addressed this transition of the RBP system using one-dimensional envelope equations. In particular, the transition from convective to absolute instability for TRs has been found (Müller *et al.* 1992) to be distinct from the stability boundary. This means for instance that, when the Rayleigh number is increased at a fixed Reynolds number, there exists a finite interval of $\mathscr{R}$ for which the RBP system is convectively unstable before it becomes abolutely unstable.

Using a set of two coupled envelope equations for TRs and LRs, convective–absolute transitions have been predicted for both roll orientations at different values of the critical parameters (Brand, Deissler & Ahlers 1991; Müller, Tveitereid & Trainoff 1993; Tveitereid & Müller 1994; Li, Kelly & Hall 1997). While the equations studied by Brand *et al.* (1991) are of a generic type, Müller *et al.* (1993) derived their equations in a systematic way. Problems arose however with the weakly nonlinear formulation, since $\mathscr{R}_c$ is different for LRs and TRs when $R > 0$. The problem was overcome by including lateral free-slip boundaries to push up $\mathscr{R}_c$ for the LRs, and by introducing in a somewhat artificial manner a Reynolds number $R^\star$ for which

the critical values of the Rayleigh number are the same for both roll orientations. This allowed $R^\star$ to be adjusted such as to reproduce some experimental results of Ouazzani *et al.* (1990).

In the present study we analyse the impulse response in the horizontal plane without restrictions on the wave propagation direction, roll orientation and control parameters, except for a restriction to low Reynolds numbers in order to avoid dealing with Tollmien–Schlichting modes. After formulating the problem in § 2, different solution approaches are discussed in § 3. In § 4, finally, our results are presented and discussed, in particular the results obtained with an approximate analytic dispersion relation, the asymptotic impulse response of the RBP system which shows that the mode with zero group velocity in all horizontal directions is always a TR mode while LRs never become absolutely unstable, the detailed roll pattern within the wave packet and a discussion of the relation of our results to various experiments.

2. Formulation of the problem

We consider a fluid layer of depth h in the vertical z-direction, with $z = 0$ at the centre of the layer and gravity pointing in the negative z-direction, and of infinite extent in the horizontal (x, y)-plane. In the following, we assume that the horizontal walls bounding the fluid are differentially heated so that the temperature is $T_0 + \delta T/2$ and $T_0 - \delta T/2$ ($\delta T > 0$) at the lower and upper walls respectively. Furthermore, we assume that a mean pressure gradient in the x-direction is maintained in the fluid layer. With the usual Boussinesq approximations, this problem of mixed convection is governed by

$$\nabla \cdot \boldsymbol{U} = 0, \tag{2.1a}$$

$$\frac{\partial \boldsymbol{U}}{\partial t} + \boldsymbol{U} \cdot \nabla \boldsymbol{U} + \frac{1}{\rho_0} \nabla \Pi - \alpha_0 (T - T_0) g \boldsymbol{e}_z - \nu_0 \nabla^2 \boldsymbol{U} = 0, \tag{2.1b}$$

$$\frac{\partial T}{\partial t} + \boldsymbol{U} \cdot \nabla T - K_0 \nabla^2 T = 0, \tag{2.1c}$$

where $\boldsymbol{e}_z$ is the unit vector in the z-direction and $\boldsymbol{U}$, Π and T are the velocity, the deviation from the hydrostatic pressure corresponding to a uniform density ρ_0 and the temperature fields respectively. The physical constants ρ_0 (density), α_0 (thermal expansion coefficient), g (gravitational acceleration), ν_0 (kinematic viscosity), and K_0 (thermal diffusivity) are assumed to be constant. The boundary conditions at the horizontal walls are

$$\boldsymbol{U} = 0 \quad \text{at} \quad z = \pm \tfrac{1}{2} h, \tag{2.2a}$$

$$T = T_0 \mp \tfrac{1}{2} \delta T \quad \text{at} \quad z = \pm \tfrac{1}{2} h. \tag{2.2b}$$

A steady basic solution of the problem is easily found as a combination of a plane Poiseuille flow and a vertical thermal stratification, i.e.

$$\boldsymbol{U}_b = U_0 \, U_b(z) \, \boldsymbol{e}_x = U_0 \left(1 - 4 \left(\frac{z}{h} \right)^2 \right) \boldsymbol{e}_x, \tag{2.3a}$$

$$T_b = T_0 - \delta T \, \frac{z}{h}, \tag{2.3b}$$

$$\Pi_b = \Pi_0 - 8 \frac{\rho_0 \nu_0 U_0}{h} \frac{x}{h} - \tfrac{1}{2} \rho_0 \alpha_0 g \delta T h \left(\frac{z}{h} \right)^2, \tag{2.3c}$$

where U_0, T_0, δT and Π_0 are externally imposed constants. Experimentally, the primary control parameters are of course U_0 and δT.

Equations governing the linear stability of this RBP system are easily deduced (Gage & Reid 1968; Kelly 1994) from the set of equations (2.1*a–c*) by linearizing around the basic solution (2.3*a–c*). At the same time we introduce non-dimensional variables by scaling all coordinates with h, the basic velocity $\boldsymbol{U}_b$ by U_0, the perturbation velocity $\boldsymbol{u}$ by K_0/h, time by h^2/K_0, the disturbance temperature by δT and the disturbance pressure by $\rho_0 \nu_0 K_0/h^2$:

$$\nabla \cdot \boldsymbol{u} = 0, \tag{2.4a}$$

$$P^{-1}\frac{\partial \boldsymbol{u}}{\partial t} + R\,(\boldsymbol{U}_b \cdot \nabla \boldsymbol{u} + \boldsymbol{u} \cdot \nabla \boldsymbol{U}_b) + \nabla p - \mathscr{R}\,\theta\,\boldsymbol{e}_z - \nabla^2 \boldsymbol{u} = 0, \tag{2.4b}$$

$$\frac{\partial \theta}{\partial t} + RP\,\boldsymbol{U}_b \cdot \nabla \theta - \boldsymbol{u} \cdot \boldsymbol{e}_z - \nabla^2 \theta = 0. \tag{2.4c}$$

Boundary conditions for $\boldsymbol{u}$ and θ are

$$\boldsymbol{u} = 0 \quad \text{at} \quad z = \pm\tfrac{1}{2}, \tag{2.5a}$$

$$\theta = 0 \quad \text{at} \quad z = \pm\tfrac{1}{2}. \tag{2.5b}$$

The three non-dimensional parameters governing the problem are P, the Prandtl number, the Reynolds number

$$R = \frac{U_0 h}{\nu_0}, \tag{2.6a}$$

and the Rayleigh number

$$\mathscr{R} = \frac{g\alpha_0 \delta T h^3}{\nu_0 K_0}. \tag{2.6b}$$

While the definition of $\mathscr{R}$ is standard in the context of Rayleigh–Bénard convection, the reader is warned that the Reynolds number is defined differently from most publications where it is normally based on half the depth and the average velocity (see Drazin & Reid 1981, for instance).

Taking the double curl of the momentum equation and using (2.4*a*), one obtains a set of two coupled equations involving w, the vertical component of the perturbation velocity $\boldsymbol{u}$, and the temperature perturbation θ:

$$-P^{-1}\frac{\partial \nabla^2 w}{\partial t} - R\left(U_b \nabla^2 - \frac{\mathrm{d}^2 U_b}{\mathrm{d}z^2}\right)\frac{\partial w}{\partial x} + \mathscr{R}\nabla_H^2 \theta + \nabla^4 w = \mathscr{F}_w, \tag{2.7a}$$

$$\frac{\partial \theta}{\partial t} + RP\,U_b \frac{\partial \theta}{\partial x} - w - \nabla^2 \theta = \mathscr{F}_\theta, \tag{2.7b}$$

where ∇_H^2 is the horizontal Laplacian (in the x, y-plane) and $\mathscr{F}_w$ and $\mathscr{F}_\theta$ are forcing terms added for later reference. The fourth-order equation for w requires an additional boundary condition on its vertical derivatives: classically it is deduced from the continuity equation, leading to the boundary conditions for the above equations:

$$w = \frac{\partial w}{\partial z} = \theta = 0 \quad \text{at} \quad z = \pm\tfrac{1}{2}. \tag{2.8}$$

The analysis of the convective and absolute nature of the instability is based on the study of the linear response of the system to a unit impulse. According to the

definition, the impulse response satisfies the equations (2.7a, b) forced by

$$\mathscr{F}_w = \mathscr{F}_\theta = \delta(x)\,\delta(y)\,\delta(z - z_0)\,\delta(t). \tag{2.9}$$

Application of Fourier transforms in space x and y as well as in time t, according to the following definitions for $\hat{w}, \hat{\hat{w}}$ and $\hat{\hat{\hat{w}}}$ and analogous definitions for $\hat{\theta}$, $\hat{\hat{\theta}}$ and $\hat{\hat{\hat{\theta}}}$

$$\hat{w}(a, y, z, t; z_0) = \int_{-\infty}^{+\infty} w(x, y, z, t; z_0)\,\exp(-\mathrm{i}ax)\,\mathrm{d}x, \tag{2.10a}$$

$$\hat{\hat{w}}(a, b, z, t; z_0) = \int_{-\infty}^{+\infty} \hat{w}(a, y, z, t; z_0)\,\exp(-\mathrm{i}by)\,\mathrm{d}y, \tag{2.10b}$$

$$\hat{\hat{\hat{w}}}(a, b, z, \omega; z_0) = \int_{-\infty}^{+\infty} \hat{\hat{w}}(a, y, z, t; z_0)\,\exp(\mathrm{i}\omega t)\,\mathrm{d}t, \tag{2.10c}$$

with a and b the components of the wave vector in the x- and y-directions and $k^2 = a^2 + b^2$, leads to the forced equation:

$$(\mathscr{L}_1 - \mathrm{i}\,\omega\mathscr{L}_2)\,\hat{\hat{\hat{\boldsymbol{S}}}} = (1, 1)^T \delta(z - z_0) \tag{2.11a}$$

for the solution vector $\hat{\hat{\hat{\boldsymbol{S}}}} = (\hat{\hat{\hat{w}}}, \hat{\hat{\hat{\theta}}})^T$, where T denotes the transpose. The two linear operators are defined as

$$\mathscr{L}_1 = \begin{pmatrix} \mathrm{i}aR\left[U_b\left(k^2 - \dfrac{\mathrm{d}^2}{\mathrm{d}z^2}\right) + \dfrac{\mathrm{d}^2 U_b}{\mathrm{d}z^2}\right] + \left(k^2 - \dfrac{\mathrm{d}^2}{\mathrm{d}z^2}\right)^2 & -k^2\mathscr{R} \\ -1 & \mathrm{i}aRPU_b + \left(k^2 - \dfrac{\mathrm{d}^2}{\mathrm{d}z^2}\right) \end{pmatrix}, \tag{2.11b}$$

$$\mathscr{L}_2 = \begin{pmatrix} P^{-1}\left(k^2 - \dfrac{\mathrm{d}^2}{\mathrm{d}z^2}\right) & 0 \\ 0 & 1 \end{pmatrix}, \tag{2.11c}$$

and the boundary conditions for the $\hat{\hat{\hat{\ }}}$ quantities are given by (2.8).

3. Solution methods

3.1. *Formal eigenfunction expansion*

We expand $\hat{\hat{\hat{w}}}$ and $\hat{\hat{\hat{\theta}}}$ in terms of the infinite set of eigenfunctions $\hat{\hat{\hat{w}}}_n(a, b, z)$ and $\hat{\hat{\hat{\theta}}}_n(a, b, z)$ of the homogeneous part of equation (2.11a) corresponding to the eigenvalues $\omega_n(a, b)$:

$$\hat{\hat{\hat{\boldsymbol{S}}}} = \sum_n A_n(a, b, \omega; z_0)\,\hat{\hat{\hat{\boldsymbol{S}}}}_n(a, b, z), \tag{3.1}$$

The coefficients A_n are determined in standard fashion. With the usual definition of the inner product

$$\left\langle \hat{\hat{\hat{\boldsymbol{S}}}} \,\middle|\, \hat{\hat{\hat{\boldsymbol{S}}}}' \right\rangle = \int_{-1/2}^{1/2} \hat{\hat{\hat{\boldsymbol{S}}}}^T\, \overline{\hat{\hat{\hat{\boldsymbol{S}}}}'}\,\mathrm{d}z, \tag{3.2}$$

one first deduces from the homogeneous version of equation (2.11a) and the corre-

sponding adjoint homogeneous problem for the adjoint eigenvector $\hat{\hat{\boldsymbol{S}}}_n^\star = (\hat{\hat{w}}_n^\star, \hat{\hat{\theta}}_n^\star)^T$, associated with the eigenvalues $\overline{\omega}_n$, the orthogonality relation

$$\left\langle \mathscr{L}_2 \hat{\hat{\boldsymbol{S}}}_m \middle| \hat{\hat{\boldsymbol{S}}}_n^\star \right\rangle = \delta_{mn}, \tag{3.3}$$

provided the eigenvectors are normalized according to

$$\left\langle \mathscr{L}_2 \hat{\hat{\boldsymbol{S}}}_n \middle| \hat{\hat{\boldsymbol{S}}}_n^\star \right\rangle = \int_{-1/2}^{1/2} \left[P^{-1} \left(k^2 \hat{\hat{w}}_n \overline{\hat{\hat{w}}_n^\star} + \frac{\mathrm{d}\hat{\hat{w}}_n}{\mathrm{d}z} \overline{\frac{\mathrm{d}\hat{\hat{w}}_n^\star}{\mathrm{d}z}} \right) + \hat{\hat{\theta}}_n \overline{\hat{\hat{\theta}}_n^\star} \right] \mathrm{d}z = 1. \tag{3.4}$$

Multiplying now (2.11a) from the right by $\hat{\hat{\boldsymbol{S}}}_n^\star$ and using the above orthonormalization immediately yields the coefficients of the expansion

$$A_n(a, b, \omega; z_0) = \frac{F_n(a, b, z_0)}{\mathrm{i}\,(\omega_n(a, b) - \omega)}, \tag{3.5}$$

where

$$F_n(a, b, z_0) = \overline{\hat{\hat{w}}_n^\star}(a, b, z_0) + \overline{\hat{\hat{\theta}}_n^\star}(a, b, z_0). \tag{3.6}$$

After solving the problem in Fourier space, we first invert the transform in time by integrating in the complex ω-plane along a contour L which is a straight line parallel to the real ω-axis lying above all singularities of the integrand, so as to satisfy the causality condition (i.e. $\boldsymbol{S}(x, y, z, t; z_0) = 0$ for $t < 0$). Clearly, the singularities of the integrand are located at $\omega = \omega_n$. The integration for $t > 0$ is performed by closing L in the lower ω-plane (see e.g. Briggs 1964; Huerre & Monkewitz 1985) and evaluating residues. Inverting also the two spatial Fourier transforms finally leads to the Green function in physical space:

$$\boldsymbol{S}(x, y, z, t; z_0) = \frac{1}{4\pi^2} \sum_n \int_{-\infty}^{+\infty} \int_{-\infty}^{+\infty} F_n(a, b, z_0)\, \hat{\hat{\boldsymbol{S}}}_n(a, b, z) \times \exp\left(-\mathrm{i}\,(\omega_n(a, b)t - ax - by)\right) \mathrm{d}b\, \mathrm{d}a, \tag{3.7}$$

To determine the long-time behaviour of the Green function we use the method of steepest descent (Huerre & Monkewitz 1990) twice, i.e. in the a-plane and the b-plane, noting that the integration contours in the two planes are coupled (Brevdo 1991). This leads to the result that on each ray (x/t=const., y/t=const.) only the mode with group velocity (x/t, y/t) will survive as $t \to \infty$. With the definitions $\omega_n' = \omega_n - b\, y/t$ and $\omega_n'' = \omega_n' - a\, x/t$ this corresponds to finding the saddle points

$$\frac{\partial \omega_n'}{\partial b}(a, b^{(s)}(a)) = 0, \tag{3.8a}$$

and

$$\frac{\partial \omega_n''}{\partial a}(a^{(s)}, b^{(s)}(a^{(s)})) = 0, \tag{3.8b}$$

The surviving mode is given asymptotically by

$$\boldsymbol{S}(x, y, z, t; z_0) \sim \frac{-\mathrm{i}}{2\pi t} \sum_n \left(\frac{\partial^2 \omega_n'}{\partial b^2}(a^{(s)}, b^{(s)}(a^{(s)})) \frac{\partial^2 \omega_n''}{\partial a^2}(a^{(s)}, b^{(s)}(a^{(s)})) \right)^{-1/2} \times F_n(a^{(s)}, b^{(s)}(a^{(s)}), z_0)\, \hat{\hat{\boldsymbol{S}}}_n(a^{(s)}, b^{(s)}(a^{(s)}), z) \exp\left(-\mathrm{i}\omega_n''(a^{(s)}, b^{(s)}(a^{(s)}))\, t\right). \tag{3.9}$$

The determination of the asymptotic wavepacket represented by (3.9) is thus reduced to the determination of the complex frequency $\omega_n''(a^{(s)}, b^{(s)}(a^{(s)}))$ for each value of $(x/t, y/t)$. Here we must immediately recall the additional so-called pinching condition for the validity of the above asymptotics (Briggs 1964; Huerre & Monkewitz (1985); Brevdo 1991; Le Dizès *et al.* 1996). This condition implies that, as the inversion contour L in the ω-plane (parallel to the real ω-axis and above all singularities) is moved down towards the singularity ω_n, its images in the complex a- and b-planes, called spatial branches, must simultaneously pinch the inversion contours in both planes at $a^{(s)}$ and $b^{(s)}$. In other words, the spatial branches in each of the two (coupled!) planes must originate (for L high above all singularities) from the upper and lower half-planes. Otherwise they cannot pinch the inversion contours in either plane, i.e. force their deformation through the saddle points at $a^{(s)}$ and $b^{(s)}$, respectively. Furthermore, it must be verified that no singularities arise between the original inversion contours along the real a- and b-axes and the deformed contours through the saddle points.

The determination of spatial branches and the associated verification of pinching requirements in two wavenumber planes for the whole range of x/t and y/t under consideration is clearly a monumental task. Therefore, the full verification of the pinching requirements has only been carried out in a few selected cases. However, in the course of all our saddle point searches, we have not found a case in which the numerical search has not converged to an acceptable solution, i.e. a solution smoothly connected in parameter space to a fully verified pinch point. Further confirmation of the results has been obtained by a direct calculation of the Green function which is described in § 3.3.

3.2. *Numerical implementation of the eigenfunction expansion: Galerkin/collocation methods*

For the practical implementation of the analysis outlined in the previous section, a standard Galerkin method is used. With basis functions $B_{w,m}(z)$ and $B_{\theta,m}(z)$, $\hat{\hat{w}}_n$ and $\hat{\hat{\theta}}_n$ are expanded as

$$\hat{\hat{w}}_n(a,b,z) = \sum_{m=0}^{m=M} W_{nm}(a,b) B_{w,m}(z), \tag{3.10a}$$

$$\hat{\hat{\theta}}_n(a,b,z) = \sum_{m=0}^{m=M} \Theta_{nm}(a,b) B_{\theta,m}(z). \tag{3.10b}$$

With $B_{w,m}(z) = (1-4z^2)^2 z^m$, $B_{\theta,m}(z) = (1-4z^2)z^m$ the 1-mode truncation of the expansions (3.6) with $M = 0$ yields a surprisingly accurate analytical approximation of the dispersion relation

$$\begin{aligned}\mathscr{D}(\omega,a,b) &= -\frac{27}{4}k^2\mathscr{R}P + (7\omega - 6aRP + 7\mathrm{i}f_1)\left(-f_2\omega + \tfrac{2}{11}aRPf_3 - \mathrm{i}Pf_4\right)\\ &= 0,\end{aligned} \tag{3.11}$$

where the f are polynomials of $k^2 = a^2 + b^2$ defined as

$$\begin{aligned} &f_1(k^2) = k^2 + 10,\ f_2(k^2) = k^2 + 12,\\ &f_3(k^2) = 5k^2 + 22,\ f_4(k^2) = k^4 + 24k^2 + 504.\end{aligned} \tag{3.12}$$

This result represents an extension of the approximate dispersion relation of Man-

neville (1991) to $R > 0$ and is of course only valid for the basic roll mode which is even in z. It will be exploited and compared to Müller's small-R expansions (Müller 1990; Müller *et al.* 1992) in §4. Higher numerical accuracy is achieved with $B_{w,m}(z)$ and $B_{\theta,m}(z)$ taken as Chebyshev polynomials $T_m(z)$. The discretized dispersion relation is obtained using a collocation method. It has the general form analogous to (2.11a)

$$\left(\mathscr{L}_1^{(d)}(a,b) - \mathrm{i}\,\omega_n(a,b)\mathscr{L}_2^{(d)}(a,b)\right)\boldsymbol{S}_n^{(d)}(a,b) = 0, \tag{3.13}$$

where $\boldsymbol{S}_n^{(d)}(a,b)$ is a vector with the $2M$ components $\{W_{nm}(a,b),\, m = 1,\dots M\}$ and $\{\Theta_{nm}(a,b),\, m = 1,\dots M\}$, while $\mathscr{L}_1^{(d)}(a,b)$ and $\mathscr{L}_2^{(d)}(a,b)$ are two $2M \times 2M$ matrices which depend implicitely on the Rayleigh, Reynolds and Prandtl numbers. For $M = 20$, we recover the classical results $\mathscr{R}_c^{(RB)} = 1707.76$ and $k_c^{(RB)} = 3.11632$.

For each $(x/t,\, y/t)$ the saddle point $(\omega_n''^{(s)},\, a^{(s)},\, b^{(s)})$ defined by (3.8a,b) is determined by a Newton method. In most cases, only the lowest mode $n = 1$ is of interest as Im $(\omega_2'') <$ Im (ω_1'') (mostly Im $(\omega_2'') < 0$).

As mentioned before, only saddle points (3.8a,b) are relevant which correspond to simultaneous (in the a- and b-planes) pinch points of spatial branches coming from the upper and lower half-planes. This requirement has been checked for selected parameters. Examples are shown on figures 1 and 2. As may be seen on figure 1(a), there exist two conjugate pinch-points corresponding to Im $(\omega_1'') \approx -0.766$ and the spatial branches are symmetric with respect to the imaginary axis. This is due to the fact that at this specific location $x/t = y/t = 0$ the dominant absolute mode in the wave packet is a TR with $b^{(s)}(a^{(s)}) = 0$. Despite the complexity of the branch structure, it is evident that the pinching criterion is satisfied in this case, as the two spatial branches are located above and below each pinch point for Im $(\omega_1'') > -0.766$ and move completely into their respective half-planes for sufficiently large values of Im (ω_1''). We also note the usual exchange of branch identities as the ω-contour is lowered to Im $(\omega_1'') < -0.766$.

In figure 1(b), on the other hand, the dominant mode is almost a LR with $a^{(s)} \approx -0.0223 - \mathrm{i}\,0.00389$ and $b^{(s)}(a^{(s)}) \approx -3.17 + \mathrm{i}\,0.44$: the spatial branches pinch for a small positive value of Im $(\omega_1'') \approx 5 \times 10^{-3}$. For Im $(\omega_1'') > 5 \times 10^{-3}$ the spatial branches are almost entirely in the left upper and in the right lower half-spaces, respectively, thus satisfying the pinching criterion. The figure suggests that, for a exactly zero, the spatial branches are symmetrically located in opposite quadrants of the b-plane with the pinching branches on the real and imaginary axes. In the present study we have however not 'hunted' for such a pure LR case away from the x/t-axis.

Finally, another way of following the pinching process is to vary the control parameter $\mathscr{R}$ as shown on figure 2. In this case we have used the analytic dispersion relation (3.11) to show its quality (compare with figure 1(a) obtained with the Galerkin expansion).

3.3. *Direct integration of the inverse Fourier transforms*

To check the validity of the preceeding asymptotics, a direct numerical integration of the Fourier transforms defined by equation (3.7) has been performed. To this end, the value of $\omega_1(a,b)$ is computed on a uniform grid in the plane of *real* wavenumbers a,b. Only the first, fastest growing mode is retained as we are interested in the asymptotic behaviour of the Green function. Moreover, it is possible to restrict the infinite integration domain to a finite a,b domain corresponding to positive Im $(\omega_1(a,b))$. The numerical integration is then performed as two one-dimensional integrals using the D01GAF routine of the NAG library for each set of x, y and t.

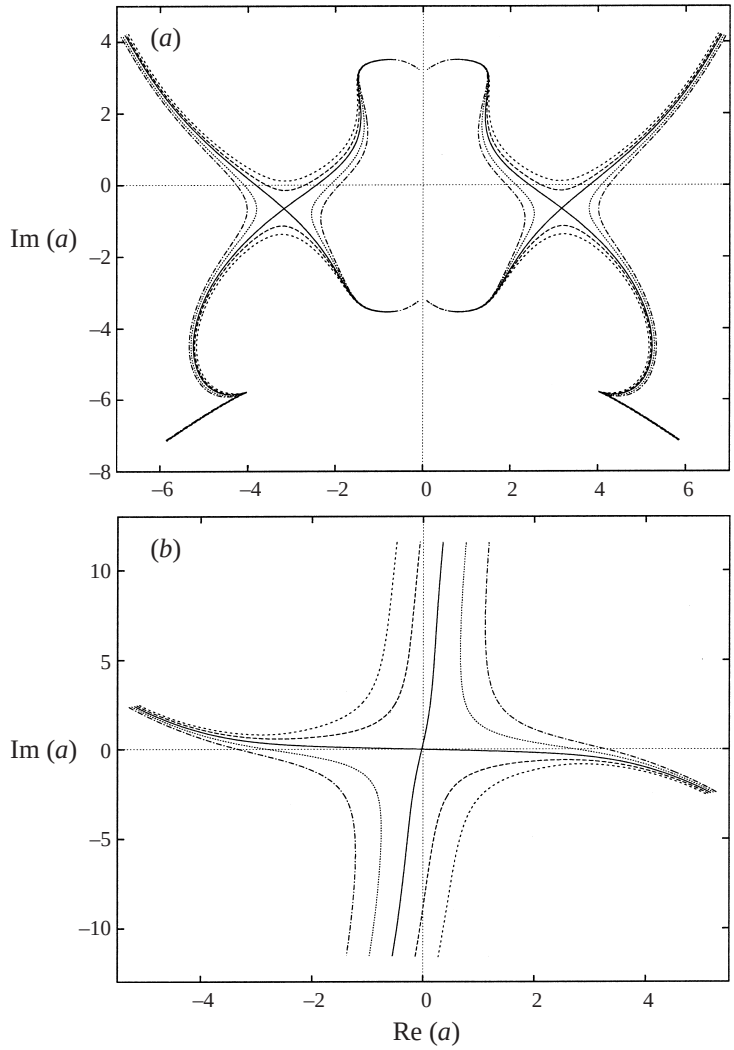

FIGURE 1. Simultaneous pinching of spatial TR-branches in the plane of complex wavenumber a under the constraint (3.8a) versus Im (ω_1'') for $P = 7$, $R = 0.63$ and $\mathscr{R} = 1760$. Group velocities are: (a) $x/t = y/t = 0$, (b) $x/t = 3.8$, $y/t = 2.5$. Dashed lines represent spatial branches for Im $(\omega_1'') >$ Im $(\omega_1''^{(s)})$; dotted and dot-dashed lines represent spatial branches for Im $(\omega_1'') <$ Im $(\omega_1''^{(s)})$.

We note, however, that this approach has a serious limitation: at a $(x/t, y/t)$ inside the growing response, the computation can only be performed for a finite time before the numerical error becomes dominant. For locations where the packet decays, the decaying nature of the impulse response results from the cancellation of exponentially growing contributions to the integrals. As a consequence, as time increases, the ratio of the impulse response to the largest contribution falls below the 'machine epsilon' and a complete loss of accuracy results which is dependent on the a and b grid sizes. Hence this method becomes rapidly unusable for large Rayleigh numbers where the exponential growth rate of unstable modes is large. To stay away from this limitation, the grid independence of the results has consistently been checked in the present

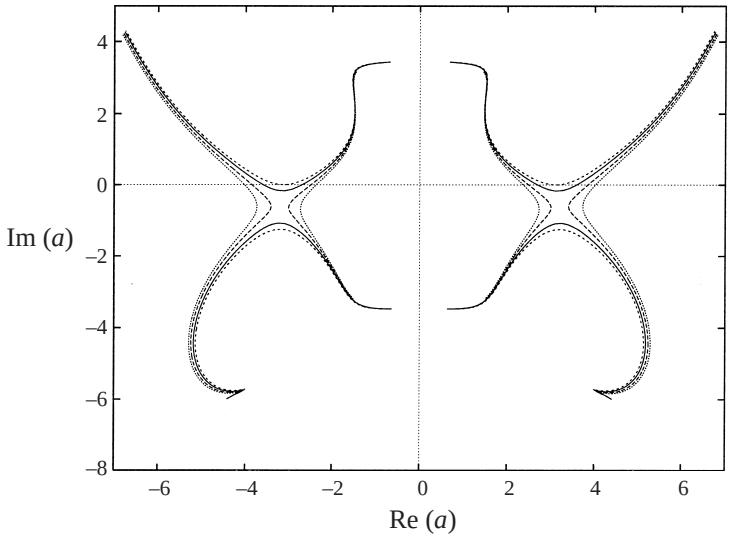

FIGURE 2. Spatial branches of the analytic dispersion relation (3.11) in the complex a-plane, constrained by (3.8a) for $P = 7$, $R = 0.63$, $x/t = y/t = 0$ and Rayleigh numbers: $\mathscr{R} = 1750$ (short dashes); $\mathscr{R} = 1803$ (solid line); $\mathscr{R} = 1874$ (dashed line); $\mathscr{R} = 1936$ (dotted line). These values of $\mathscr{R}$ correspond to the same supercriticality ($\mathscr{R}/\mathscr{R}_c^{(RB)} - 1$) as $\mathscr{R} = 1708$, 1760, 1828 ($\approx \mathscr{R}_a$) and 1890 in the exact problem.

study. Also, the time required for establishing the asymptotic growth rate was found to be always sufficiently small.

4. Results

4.1. *Analytical stability boundaries*

From the approximate analytical dispersion relation (3.11) with $R = 0$ and $\omega = 0$, one immediately obtains the marginal Rayleigh number $\mathscr{R}^{(RB)}$ for pure Rayleigh–Bénard convection as

$$\mathscr{R}^{(RB)}(k^2) = \frac{28}{27}\frac{f_1 f_4}{k^2}. \tag{4.1}$$

The critical wavenumber $k_c^{(RB)} = 3.1165$ is obtained as the real solution of $\partial\mathscr{R}^{(RB)}/\partial k^2 = 0$ and is very close to the exact value. The corresponding $\mathscr{R}^{(RB)}(k_c^2) = \mathscr{R}_c^{(RB)} = 1749.98$ is however 2.5% higher than the exact value (Manneville 1991). A quick inspection of (3.11) shows that the same critical parameters also apply to longitudinal rolls ($a = 0, k = b$) in the RBP system, which is of course well known.

From (3.11) it is also straightforward to deduce the characteristics of the marginal state for $R > 0$ and transverse rolls ($b = 0, k = a$):

$$\omega^{(TR)}(a, R, P) = \tfrac{6}{7} aRP\frac{Pf_4 + (7/33)f_1 f_3}{Pf_4 + f_1 f_2} \equiv aRPF(k^2), \tag{4.2}$$

and

$$\mathscr{R}^{(TR)}(k^2, R, P) - \mathscr{R}^{(RB)}(k^2) = \tfrac{4}{27} R^2 P\, \Phi(k^2, P), \tag{4.3a}$$

$$\Phi(k^2, P) = \left[7F(k^2) - 6\right]\left[-f_2 F(k^2) + (2/11)f_3\right], \tag{4.3b}$$

with $\mathscr{R}^{(RB)}$ given by (4.1) and $F(k^2)$ by (4.2). The critical wavenumber is obtained from $\partial \mathscr{R}^{(TR)}/\partial k = 0$ and can be written as

$$k_c^{2(TR)} = k_c^{2(RB)} - R^2 P \varphi(R, P).$$

Retaining only linear terms in $R^2 P \varphi$, one obtains

$$\varphi(R, P) \approx \Phi'|_{k_c^{(RB)}} \left[\tfrac{27}{4} \mathscr{R}^{(RB)''}\big|_{k_c^{(RB)}} + R^2 P \Phi''|_{k_c^{(RB)}} \right]^{-1}, \tag{4.4}$$

where primes denote derivatives with respect to k^2. We note that, for small Prandtl numbers, the critical wavenumber depends only weakly on Reynolds number and the phase speed of the critical TR is therefore nearly proportional to R. For large P, on the other hand, k_c depends markedly on R and the behaviour of the critical phase speed is more complicated.

These results may be compared to the small-R expansions of Müller (1990) and Müller *et al.* (1992), noting that the latter were obtained by expanding the solution of the full linear problem (the homogeneous version of equation (2.11*a*)) in powers of R and truncating at the lowest non-trivial order, while the derivation of our analytical results does not involve any small-R expansion (except for equation (4.4)). Their approximate nature is entirely due to the projection of the solution, defined by the equations (3.10*a*, *b*), onto only one pair of approximate eigenfunctions. For k fixed to $k = k_c^{(RB)}$, Müller has numerically fitted the low-R approximation of the marginal TR frequency with

$$\omega^{(TR)}(k_c^{(RB)}, P, R) = RP \frac{2.7367P + 0.9393}{P + 0.5117}, \tag{4.5}$$

and found the corresponding approximate $\mathscr{R}_c^{(TR)}$ to be within 1% of the exact value in the range $RP < 40$. For comparison, we obtain from (4.2)

$$\omega^{(TR)}(k_c^{(RB)}, P, R) = RP \frac{2.6713P + 0.9480}{P + 0.5148}, \tag{4.6}$$

which displays the same functional dependence on R and P as Müller's fit and is numerically close. The corresponding $\mathscr{R}^{(TR)}(k_c^{(RB)}, P, R) - \mathscr{R}_c^{(RB)}$ obtained from (4.3) is also in excellent agreement with Müller (1990).

4.2. *The evolution of the wavepacket and transition to absolute instability*

In the following, we restrict ourselves to Rayleigh numbers $\mathscr{R} > \mathscr{R}_c$ for which there exists a region of the wave packet with positive growth rate Im (ω_n''). In the context of (3.9), we have to determine the region of positive values of Im (ω_n'') in the plane $(x/t, y/t)$. If this region includes the origin, then the instability is absolute, otherwise it is convective. Figure 3, computed for $P = 7$ and $R = 0.63$, shows a typical evolution of the region Im $(\omega_1''^{(s)}) \geqslant 0$ as $\mathscr{R}$ is increased. The complex wavenumbers $a^{(s)}$ and $b^{(s)}$, not shown in the figure, evidently vary along the isocontours of Im $(\omega_1''^{(s)})$. In figure 3(*a*) the instability is clearly convective, i.e. $\mathscr{R}_c < \mathscr{R} < \mathscr{R}_a$ where $\mathscr{R}_a(P, R)$ denotes the transition to absolute instability. Figure 3(*b*) shows a marginally absolutely unstable case with $\mathscr{R} = \mathscr{R}_a$ where the absolute growth rate Im $(\omega_1''^{(s)}) = 0$ at $x/t = y/t = 0$. Figure 3(*c*), finally, shows an absolutely unstable situation $\mathscr{R} > \mathscr{R}_a$ where the origin lies within the unstable disc and part of the wave packet moves upstream. We note that between figures 3(*a*) and 3(*c*) the size of the disc with Im $(\omega_1''^{(s)}) > 0$ increases, while its centre, corresponding to the location where Im $(\omega_1''^{(s)})$ is equal to the maximum temporal growth rate which is attained for longitudinal rolls ($a = 0$), remains nearly fixed.

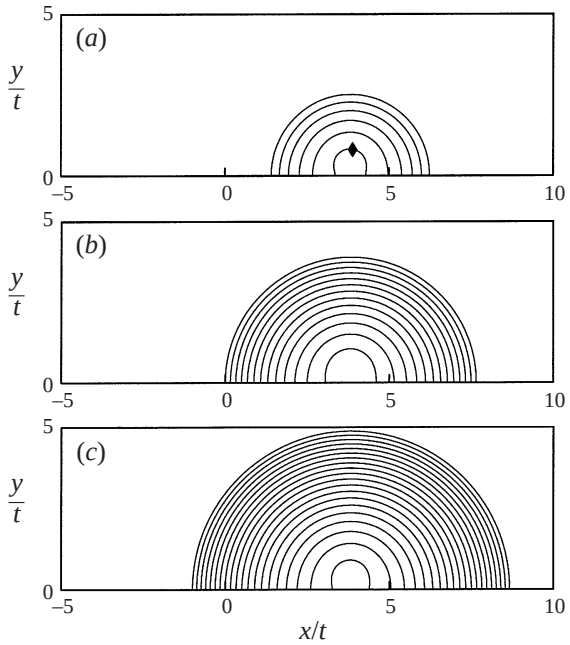

FIGURE 3. Isocontours (in increments of 0.1) of positive Im $(\omega_1^{\prime\prime(s)})$ (the outermost contour corresponds to zero growth rate) in the plane $(x/t, y/t)$ for $P = 7$, $R = 0.63$ and different Rayleigh numbers. (a) $\mathscr{R} = 1760$ (the contour marked by ◆ corresponds to the similarly marked contour of figure 6b); (b) $\mathscr{R} = 1827.93 \approx \mathscr{R}_a$; (c) $\mathscr{R} = 1890$.

x/t	y/t	$\omega_1^{\prime\prime(s)}$ (AS)	$\omega_1^{\prime\prime(s)}$(DI)
0	0	$11.9 - \mathrm{i}\,0.766$	$12.0 - \mathrm{i}\,0.827$
1.41	0	7.47	$7.48 - \mathrm{i}\,0.0617$
3.8	0	$\mathrm{i}\,0.547$	$\mathrm{i}\,0.507$
6.24	0	−7.79	$-7.72 - \mathrm{i}\,0.06$
3.8	2.51	7.88	$7.94 - \mathrm{i}\,0.0575$

TABLE 1. Comparison of absolute frequencies obtained by asymptotic method (AS) and direct integration (DI) of Fourier transforms.

The accuracy of these results, obtained with the Chebyshev collocation method, was checked by direct integration of the inverse Fourier transforms. A comparison at five points of the $(x/t, y/t)$-plane of figure 3(a) is given in table 1. As a further check, it was verified that the graphs of figure 3 are recovered within 'drawing accuracy' when using the approximate analytic dispersion relation (3.11) to determine Im $(\omega_1^{\prime\prime(s)})$, provided the same supercriticality parameter $\mathscr{R}/\mathscr{R}_c - 1$ is chosen to compensate for the high value of $\mathscr{R}_c$ obtained from (3.11).

To investigate the roll orientation corresponding to the absolute mode at $x/t = y/t = 0$, we note that, on $y/t = 0$, the condition (3.8a) together with the symmetry $y \to -y$ limits the possible solutions to either $b = 0$ or b real and a pure imaginary. In our computations we find that it is always the transverse roll solution ($b = 0$) which has the highest absolute growth rate at $x/t = y/t = 0$. This means that the boundary of absolute instability $\mathscr{R}_a$ in the general case with two wave propagation

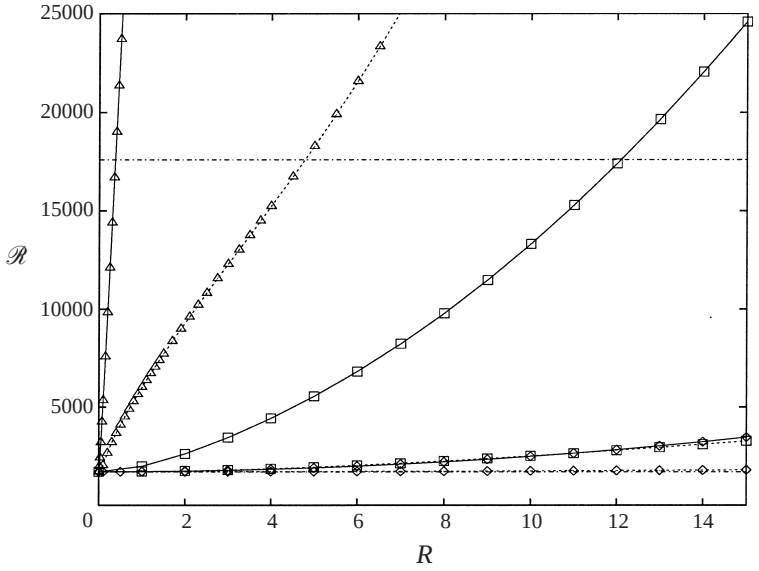

FIGURE 4. Critical Rayleigh number $\mathscr{R}_c^{(TR)}$ (dashed lines) and convective–absolute transition $\mathscr{R}_a^{(TR)}$ (solid lines) for TRs versus Reynolds number with: $P = 0.71$ ($\diamond$), $P = 7$ ($\square$), $P = 450$ ($\triangle$). Horizontal dot-dashed lines without symbols represent $\mathscr{R}_c^{(LR)}$ for the first (lower line) and for the second LR-mode (upper line).

directions coincides with the absolute instability boundary $\mathscr{R}_a^{(TR)}$ for transverse rolls (Müller 1990).

The dependence of the absolute Rayleigh number $\mathscr{R}_a$ on the Reynolds number is therefore determined by TRs and is shown on figure 4 for three values of P: 0.71 (air as in the experiment of Ouazzani *et al.* 1989), 7 (water, experiment of Ouazzani *et al.* 1990) and 450 (silicon oil, experiment of Luijkx *et al.* 1981). For small Reynolds numbers and moderate P, $\mathscr{R}_a - \mathscr{R}_c^{(RB)}$ is seen to be very nearly proportional to R^2. This is consistent with the analytical relation (3.11) which, when expanded for small R in the manner of §4.1, yields a proportionality to R^2P times a weak function of P. For larger R, the difference between $\mathscr{R}_a$ and $\mathscr{R}_c^{(TR)}$ increases rapidly. With $P = 7$, for instance, at $R \approx 11.8$ $\mathscr{R}_a$ already exceeds the stability limit of the second LR-mode, which is included on the figure for reference. For larger R^2P, $\mathscr{R}_a(R)$ deviates more and more from the leading-order parabolic behaviour, most markedly for the highest Prandtl number of 450, but remains a monotonically increasing function of R. This agrees qualitatively with the results of Müller *et al.* (1992) based on an amplitude equation for TRs.

Returning to the question of the stability characteristics of longitudinal rolls, we need to elucidate the obvious contradiction between our numerical finding that LRs represent a convective instability for all $R > 0$ and the results of Brand *et al.* (1991), Müller *et al.* (1993), Kelly (1994) (his figure 12), Tveitereid & Müller (1994) and Li *et al.* (1997) who deduced a convective–absolute transition $\mathscr{R}_a^{(LR)}(R)$ from amplitude equations. This clarification is best done with the help of the approximate analytic dispersion relation (3.11).

In the following we can restrict the analysis to the axis $y/t = 0$ so that ω in (3.11) can be replaced by $\omega'' + a\,x/t$, according to the definitions of §3.1. Since b appears only in k^2, the condition (3.8*a*) of zero transverse group velocity implies

$\partial\mathscr{D}/\partial b = 2b\partial\mathscr{D}/\partial k^2 = 0$. For non-transverse rolls ($b \neq 0$), the condition (3.8b), thus reduces to

$$\left(\frac{x}{t} - \tfrac{6}{7}RP\right)\left[-f_2\omega'' + a\left(-f_2\frac{x}{t} + \tfrac{2}{11}RPf_3\right) - \mathrm{i}Pf_4\right] + \left(-f_2\frac{x}{t} + \tfrac{2}{11}RPf_3\right)\left[\omega'' + a\left(\frac{x}{t} + \tfrac{6}{7}RP\right) + \mathrm{i}f_1\right] = 0. \quad (4.7)$$

In the case of purely longitudinal rolls, we must have Re (a) = 0. Moreover, it can be shown that, according to the symmetry of the problem, b is real, implying that $k^2 = b^2 - \mathrm{Im}(a)^2$ is also real and that ω'' is pure imaginary. A first result for the location of the centre of the wave packet is easily obtained for the special case $\mathscr{R} = \mathscr{R}_c^{(RB)}$. In this case it follows from (3.11) and (4.7) that

$$a = \omega'' = 0, \quad b = k_c^{(RB)} \quad (4.8a)$$

and

$$\left.\frac{x}{t}\right|_{\text{centre}}(\mathscr{R}_c^{(RB)}) = \tfrac{6}{7}RP\,\frac{P + 0.3549}{P + 0.5147}, \quad (4.8b)$$

which is strictly positive for $R > 0$. To show that LR modes on $y/t = 0$ have a positive velocity, we seek two points ($x/t|_{+/-} > 0, y/t = 0$) with $k^2 = 0$ on either side of $x/t|_{\text{centre}}$, where k^2 is necessarily positive. These points are

$$\left.\frac{x}{t}\right|_{+} = \tfrac{6}{7}RP > \left.\frac{x}{t}\right|_{\text{centre}}, \quad \mathrm{Im}(\omega'')|_{+} = -10 \quad (4.9a)$$

and

$$\left.\frac{x}{t}\right|_{-} = \tfrac{1}{3}RP < \left.\frac{x}{t}\right|_{\text{centre}}, \quad \mathrm{Im}(\omega'')|_{-} = -42P, \quad (4.9b)$$

independent of $\mathscr{R}$. The corresponding Im(a) are determined from $\partial\mathscr{D}/\partial k^2 = 0$. For all $\mathscr{R} \geqslant \mathscr{R}_c^{(RB)}$ and all P, these Im(a) were found to assume large positive values at $x/t|_{+}$ and large negative values at $x/t|_{-}$. A numerical survey of the x/t-axis to the right of $x/t|_{+}$ and left of $x/t|_{-}$ has furthermore shown that Im(ω'') remains negative for the entire extensive range of $\mathscr{R}$, R and P which was surveyed. As the point $x/t = 0$ lies to the left of $x/t|_{-}$, this analysis of the approximate dispersion relation (3.11) fully agrees with our conclusion that LRs never represent an absolute instability if $R > 0$. In other words, the absolute instability boundary for LRs in the $(\mathscr{R}, R)$-plane is the axis $R = 0$.

The above analytical results also point to the probable cause of the erroneous prediction of absolutely unstable LR-modes by amplitude equations. The latter have all been obtained with a scaling that implies a slow variation (on the scale of the transverse wavelength) of the roll amplitude along the roll direction, i.e. along x. While this is appropriate in the immediate vicinity of the wave-packet centre, where $a = 0$, we have found that the streamwise growth or decay rates $\mp\mathrm{Im}(a)$ are large away from the centre, in particular at $x/t = 0$, which implies fast streamwise variations of the roll amplitude. We therefore believe that the results of Müller *et al.* (1993), Kelly (1994), Tveitereid & Müller (1994) and Li *et al.* (1997) pertaining to the absolute instability boundary for LRs are the result of the amplitude equations in question being used outside their range of validity.

4.3. *The roll pattern within the wave packet*

To further clarify the roll pattern within the asymptotic wave packet, the shape of the wave packet at a fixed time is shown in figure 5, where the value of $w(x, y, z_0, t; z_0)$ is

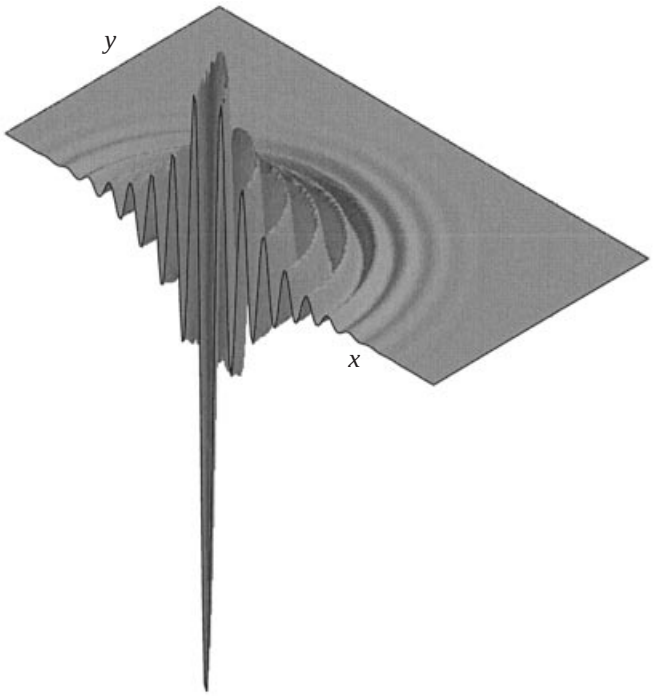

FIGURE 5. View of the wave packet in terms of $w(x, y, z_0, t)$ in the region of the (x, y)-plane delimited by $0 \leqslant x \leqslant 40$, $0 \leqslant y \leqslant 20$ at $t = 5$ for the parameters $P = 7$, $R = 0.63$, $\mathscr{R} = 1760$.

plotted in the (x, y)-plane. This example, computed by direct inversion of the Fourier transforms, happens to be a convective case but the roll pattern is hardly affected by the value of $\mathscr{R}$. It is obvious from figure 5 that the wave packet consists of circular rolls around its centre. We note however, that the roll amplitude is not uniform on each circle, particularly near the centre where the packet grows lateral 'ears' which correspond to a locally higher growth rate. Since the direct inversion of the Fourier transforms is limited to relatively small times, the wave packet of figure 5 contains only few rolls, which does not permit the pattern close to the centre to be resolved. We therefore proceed to a zoom of the wave-packet centre in figure 3(a) which is shown as figure 6. In this zoom, the isophase lines of the wave packet are still circular, but the iso-growth lines take the shape of 'light bulbs' near the centre. This explains the 'ears' in figure 5. As time progresses, the amplitude in the 'ears' of a circular roll becomes exponentially larger than its amplitude on the axis $y/t = 0$ and in an experiment we expect to see a roll pattern emerge in the form of the 'lighthouse' pattern sketched in figure 7. We speculate that such 'lighthouse' patterns can merge and synchronize via nonlinear interactions to form the LRs often observed in experiments.

While figure 6 explains the 'ears' of the roll pattern, it still does not resolve the very centre, where we expect to find the most amplified temporal mode, namely a LR. A further zoom, shown in figure 8, finally provides the detailed picture accompanied, as usual, by some questions.

Figure 8(a) shows that in a small x/t-interval around $x/t|_{\text{centre}}$ LRs do prevail over TRs, which still exist in this interval but have a smaller growth rate $\mathrm{Im}(\omega'')$ than the LRs. This interval on figure 8(b) is bounded by two vertical lines at $x/t \approx 3.76$ and $x/t \approx 3.81$ which correspond to points where the growth rate of a mode smoothly

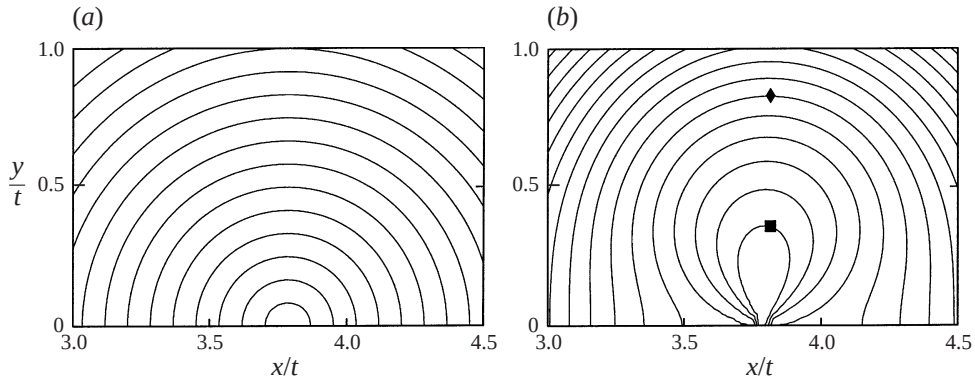

FIGURE 6. Isocontours of (*a*) Re $(\omega_1^{\prime\prime(s)})$ (increments of $\pi/12$) and (*b*) Im $(\omega_1^{\prime\prime(s)})$ (increments of 0.01) in the vicinity of the centre of the wave packet for $P = 7$, $R = 0.63$, $\mathscr{R} = 1760$. The symbol ◆ marks the contour Im $(\omega_1^{\prime\prime(s)}) = 0.5$ corresponding to figure 3(*a*) and ■ establishes the correspondence to the further zoom in figure 8(*b*).

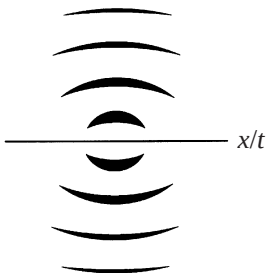

FIGURE 7. Sketch of the expected 'lighthouse' roll pattern near the centre of the wave packet.

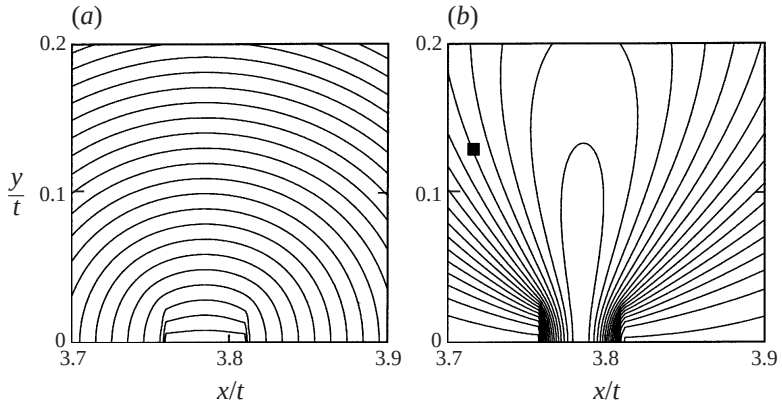

FIGURE 8. Further zoom of figure 6 for the same parameter values. Contour lines in increments of $\pi/96$ for Re $(\omega_1^{\prime\prime(s)})$ (*a*) and 0.0025 for Im $(\omega_1^{\prime\prime(s)})$ (*b*). The symbol ■ marks the contour Im $(\omega_1^{\prime\prime(s)}) = 0.55$ corresponding to figure 6(*b*).

connected to pure LRs at the centre is equal to the growth rate of a mode smoothly connected to pure TRs. These two lines appear to 'end' at $y/t \approx 0.026$, and beyond this y/t the isophase lines are smoothly connected. One is therefore led to speculate that the 'ends' correspond to the coalescence of the two above mentioned modes but,

owing to limited numerical accuracy, we have not been able to untangle the complex spatial branch structure near these points.

Figure 8(*b*) also confirms that the maximum growth rate within the packet is indeed associated with the temporally most amplified LR on the x/t-axis. For times much longer than shown on figure 5, we therefore expect that a spanwise extended region of LRs dominates the rest of the wave packet. It is interesting to estimate the time t^* necessary for this central region of LRs to attain a dimensional streamwise extent of, say, $10h$. From the non-dimensional $\Delta x/t \approx 0.05$ we obtain $t^* U_0/h = 200RP$. This result suggests that, at least for the present parameters, one needs a very large cell to grow this central LR-region. Furthermore it is clear that, for any $\mathscr{R}$ significantly larger than $\mathscr{R}_c^{(RB)}$, nonlinear effects will become important long before this region develops to an observable size.

4.4. *Discussion of the results in relation to experiments*

To our knowledge, none of the laboratory experiments reported in the literature can be directly compared with our results. Clearly, the presence of an inlet, outlet and sidewalls, which we have not considered, is important. Equally or more important is the level and nature of external perturbations imposed on the RBP cell, which are generally not documented in experimental papers (they would also be very difficult to measure). Therefore we are limited to an interpretation of experimental findings in terms of the convective and absolute nature of LRs and TRs.

As long as the flow is only convectively unstable, i.e. $\mathscr{R} < \mathscr{R}_a$, and the cell aspect ratio (its width) is sufficiently large, we expect that any reasonably random low-level inlet perturbation generates a succession of growing wave packets which are convected downstream, with nonlinear effects becoming effective relatively far from the inlet (cf. Tveitereid & Müller 1994). According to the discussion of roll pattern selection in § 4.3, one should observe mostly longitudinal rolls sufficiently far from the inlet. This argument is of course based on linear concepts and we cannot exclude complicated nonlinear effects leading to a different pattern. Nevertheless, the linear scenario is supported by the study of Fukui *et al.* (1983) carried out in a cell of large aspect ratio (19.5) with air ($P = 0.71$) as test fluid. They made observations in a cross-section far downstream (73 hydraulic diameters) of the inlet and observed only LRs for a range of $\mathscr{R}$ and R where, according to our results, the instability is always convective.

When, on the other hand, $\mathscr{R}$ exceeds the absolute instability boundary $\mathscr{R}_a$, the appearance of self-excited TRs is already expected near the inlet of the RBP cell. This is confirmed by comparing with the two-dimensional numerical experiments of Nicolas, Mojtabi & Platten (1997). In their figure 12 they distinguish in the $(\mathscr{R}, R)$-plane between points where TRs were detected in a computational cell of finite length L ($L = 10h$ and $20h$) without applying any forcing, and points where only pure Poiseuille flow was observed. They found the boundary between no TRs and TRs to fall somewhat below the curve $\mathscr{R}_a(R)$ determined from the amplitude equation of Müller (1990). Actually, as shown on figure 9, the results of Nicolas *et al.* (1997) line up almost perfectly with the exact $\mathscr{R}_a(R)$ curve for $P = 6.4$ (note the factor 1.5 between their Re and our R).

Probably the best laboratory experiment to test the expectation of finding TRs for $\mathscr{R} > \mathscr{R}_a$, is the one by Ouazzani *et al.* (1989) who worked with an aspect ratio of 19.5 and air. Raising R for different fixed values of $\mathscr{R}$, the authors observed a transition from TRs to LRs. The roll orientation was identified by simultaneously visualizing the flow in the (x, z)- and a (y, z)-plane (located at an unspecified x) with the help of two laser sheets. At low Reynolds numbers, the TRs appeared close to the inlet, which is

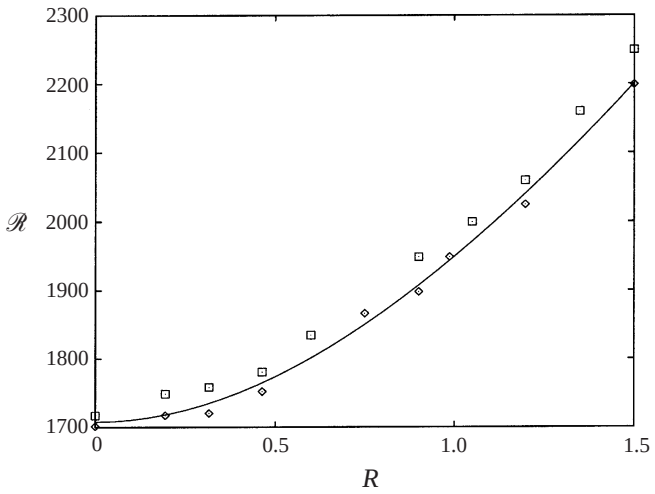

FIGURE 9. The numerically observed transition from Poiseuille flow (◇) to TRs (□) adapted from figure 12 of Nicolas *et al.* (1997) in relation to the curve of marginal absolute instability (solid line) for $P = 6.4$.

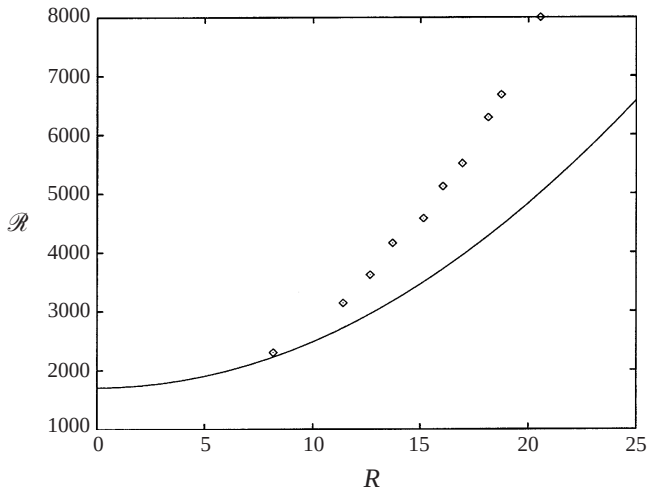

FIGURE 10. Comparison between the TR–LR transition observed experimentally by Ouazzani *et al.* (1989) (◇) and the curve of marginal absolute instability (solid line) for $P = 0.71$.

consistent with an absolutely instability. As R was raised, the TRs developed spanwise modulations and, eventually, a clear LR pattern emerged in the entire cross-section. This experimentally observed TR–LR transition is reproduced in figure 10, together with the theoretical convective–absolute boundary $\mathscr{R}_a(R)$ for $P = 0.71$ from figure 4. The experimental TR–LR transitions in figure 10 clearly take place in the region where the infinite RBP system is absolutely unstable with respect to TRs, which is consistent with our pattern selection scenario. The experimental transition curve and the curve $\mathscr{R}_a(R)$ also exhibit a qualitative similarity, but it must be emphasized that the experimental points represent transitions between *fully developed* TRs and LRs where nonlinear effects are certainly not negligible. Moreover, it is not entirely clear from the paper of Ouazzani *et al.* (1989) whether at the transition point the TRs

disappeared everywhere in the cell or whether they persisted longer near the inlet, for instance.

A comparison with other experiments by Luijkx *et al.* (1981) and Ouazzani *et al.* (1990) is more difficult since they used small aspect ratio cells, which have considerably modified stability characteristics. Nevertheless, in both studies TRs were observed for large values of the Rayleigh number which correspond to absolute instability of the infinite RBP system. These experiments, carried out with silicon oil ($P = 450$) and water ($P = 7$), respectively, also reveal a rapid increase of the TR–LR transition Rayleigh number with increasing R, which is consistent with the strong Prandtl number dependence of $\mathscr{R}_a(R)$ in figure 4. From these generally encouraging comparisons it is clear that, in order to establish a firm and quantitative link between the present theory and experiments, more experimental work in large RBP cells with carefully controlled external perturbations is needed.

The financial support of the Swiss National Science Foundation under grant no. 21-39572.93 and of the ERCOFTAC Leonhard Euler Center (Ph.C.) are gratefully acknowledged. We also would like to thank J. F. Scott and A. Bottaro for several helpful discussions.

REFERENCES

Akiyama, M., Hwang, G. J. & Cheng, K. C. 1971 Experiments on the onset of longitudinal vortices in laminar forced convection between horizontal plates. *J. Heat Transfer* **93**, 335–341.

Brand, H. R., Deissler, R. J. & Ahlers, G. 1991 Simple model for the Bénard instability with horizontal flow near threshold. *Phys. Rev.* A **43**, 4262–4268.

Brevdo, L. 1991 Three-dimensional absolute and convective instabilities, and spatially amplifying waves in parallel shear flows. *Z. Angew. Math. Phys.* **42**, 911–942.

Briggs, R. J. 1964 *Electron-Stream Interaction with Plasmas.* Research Monograph 29. MIT Press.

Deissler, R. J. 1987 The convective nature of instability in plane Poiseuille flow. *Phys. Fluids* **30**, 2303–2305.

Drazin, P. & Reid, W. 1981 *Hydrodynamic Instability*. Cambridge University Press.

Fujimura, K. & Kelly, R. E. 1995 Interaction between longitudinal convection rolls and transverse waves in unstably stratified plane Poiseuille flow. *Phys. Fluids* **7**, 68–79.

Fukui, K., Nakajima, M. & Hueda, H. 1983 The longitudinal vortex and its effects on the transport processes in combined free and forced laminar convection between horizontal and inclined parallel plates. *Intl J. Heat Mass Transfer* **26**, 109–120.

Gage, K. S. & Reid, W. H. 1968 The stability of thermally stratified plane Poiseuille flow. *J. Fluid Mech.* **33**, 21–32.

Huerre, P. & Monkewitz, P. A. 1985 Absolute and convective instabilities in free shear layers. *J. Fluid Mech* **159**, 151–168.

Huerre, P. & Monkewitz, P. A. 1990 Local and global instabilities in spatially developing flows. *Ann. Rev. Fluid Mech* **22**, 473–537.

Kelly, R. E. 1994 The onset and development of thermal convection in fully developed shear flows. *Adv. Appl. Mech.* **31**, 35–112.

Le Dizès, S., Huerre, P., Chomaz, J. M. & Monkewitz, P. A. 1996 Linear global modes in spatially developing media. *Phil. Trans. R. Soc. Lond.* A **354**, 169–212.

Li, H., Kelly, R. E. & Hall, P. 1997 Absolute instability of Rayleigh–Bénard convection in a time-periodic shear flow. *Phys. Fluids* **9**, 1273–1276.

Luijkx, J. M., Platten, J. K. & Legros, J. C. 1981 On the existence of thermoconvective rolls, transverse to a superimposed mean Poiseuille flow. *Intl J. Heat Mass Transfer* **24**, 1287–1291.

Manneville, P. 1991 *Structures Dissipatives, Chaos et Turbulence.* Aléa Saclay.

Müller, H. W. 1990 Thermische Konvektion in Horizontaler Scherströmung. PhD thesis, Universität des Saarlandes, Saarbrücken.

Müller, H. W., Lücke, M. & Kamps, M. 1992 Transversal convection patterns in horizontal shear flow. *Phys. Rev.* A **45**, 3714–3726.

Müller, H. W., Tveitereid, M. & Trainoff, S. 1993 Rayleigh–Bénard problem with imposed weak through-flow: Two coupled Ginzburg–Landau equations. *Phys. Rev.* E **48**, 263–272.

Nicolas, X., Mojtabi, A. & Platten, J. 1997 Two-dimensional numerical analysis of the Poiseuille–Bénard flow in a rectangular channel heated from below. *Phys. Fluids* **9**, 337–348.

Ostrach, S. & Kamotani, Y. 1975 Heat transfer augmentation in laminar fully developed channel flow by means of heating from below. *J. Heat Transfer* **97**, 220–225.

Ouazzani, M. T., Catalgirone, J. P., Meyer, G. & Mojtabi, A. 1989 Etude numérique et expérimentale de la convection mixte entre deux plans horizontaux à températures différentes. *Intl J. Heat Mass Transfer* **32**, 261–269.

Ouazzani, M. T., Platten, J. K. & Mojtabi, A. 1990 Etude numérique et expérimentale de la convection mixte entre deux plans horizontaux à températures différentes–II. *Intl J. Heat Mass Transfer* **33**, 1417–1427.

Tveitereid, M. & Müller, H. W. 1994 Pattern selection at the onset of Rayleigh–Bénard convection in a horizontal shear flow. *Phys. Rev.* E **50**, 1219–1226.